Int. J. Heat Mass Transfer. Vol. 33, No. 10, pp. 2207–2217, 1990
Printed in Great Britain

0017-9310/90 $3.00 + 0.00
Pergamon Press plc

Energy considerations in high-energy beam drilling

P. S. WEI and J. Y. HO
Institute of Mechanical Engineering, National Sun Yat-Sen University, Kaohsiung, Taiwan, China

(*Received September* 1989)

Abstract—Energy transfers and penetration velocity during a high-energy drilling or welding process are determined. The beam energy of a Gaussian distribution incident on the free surface of a liquid layer that separates unmelted solid and vapour is balanced with the heat conduction and latent heats for melting and evaporation. The shapes of the vapour–liquid, the liquid–solid interfaces and the penetration velocity are determined as a function of the energy distribution and beam power. Convective heat transfer is neglected due to a small Peclet number of around 2 near the cavity bottom. Results show that non-linear variation in the penetration velocity with energy density and an evaporation rate of the order of 1×10^{-7} kg s^{-1} agree with experimental data for drilling copper. The energy required for melting or evaporation is only 2–3% of the incident energy in the range below 7×10^{10} W m^{-2}. The conventional pure evaporation one-dimensional penetration model is inherently invalid due to a significant overestimation of the evaporation rate and nearly 50% radial heat conduction loss.

INTRODUCTION

THE HIGH-energy beam (electron or laser beam) has become a widely used tool in welding, drilling and cutting. Regardless of the extremely good metallurgical quality, the high-energy metalworking process has the exceptional advantage of producing a fusion zone with high depth-to-width ratios of 5–10 or greater [1, 2]. Consequently, the total amount of material affected or distorted is reduced to a minimum.

The physical phenomena of deep penetration for the fusion zone are complicated due to rapid interactions within the incident high-energy beam, the evaporating atoms, and the flow of the liquid layer along the wall of the vapour-filled cavity produced by the high-energy beam [3, 4]. Ready [5], and Connor [6] proposed that deep penetration was associated with evaporation. A high-energy beam irradiates on the metal and raises the surface temperature to the boiling point. Due to strong evaporation a vapour-filled cavity is produced. If the energy beam continuously impinges on the cavity base, a deep and narrow cavity and a thin fusion zone are finally formed.

An alternative explanation was given in refs. [7, 8]. They interpreted a high-energy beam welding process by calculating the fluid flow of the molten metal in a thin layer around the vapour-supported cavity. The longitudinal vapour pressure variation was not taken into account. The driving force for the liquid layer flowing around the cavity wall to the rear where it cools and solidifies was found to be the increase in surface tension as the free surface temperature decreases from the forward centreline around the cavity. Although the welding process was studied under a steady-state condition, some of the physical phenomena of the drilling process can be discovered, because these steady-state processes take place on a smaller time scale compared to the movement of the workpiece relative to the high-energy beam.

Recently, an axisymmetric, quasi-steady model was developed to calculate the fluid flow of the liquid layer near the cavity base during a high-energy beam penetrating process [9]. The effective pressure, which is the sum of the gas pressure near the free surface and the pressure due to evaporation, and the force due to surface tension are the forces driving the liquid layer to flow upward. It is interesting to find that the evaporation rate calculated was only 1/200 of that due to melting. Hence, the formation of the cavity is believed to be primarily due to the melting process and upward motion of the liquid layer rather than evaporation, which has been widely accepted by most researchers working on the laser-beam drilling process.

The proposed mechanisms of penetration by pure evaporation and melting exhibit significant differences. Regardless of overestimation of the evaporation rate and the associated energy loss, the one-dimensional pure evaporation model [5, 10] is generally unable to describe the non-linear relationship observed by von Allmen [11] between the penetration velocity and the energy density. Besides, using a one-dimensional model to predict a high-energy beam drilling process is inherently invalid since significant errors occur at the cavity base where length scales are about the same in both the axial and the radial directions.

Giedt and Tallerico [12] found that the first and second priorities for precision in welding parameter are the energy distribution parameter and the beam

NOMENCLATURE

c	specific heat [J kg^{-1} K^{-1}]
f	vapour–liquid interface location as illustrated in Fig. 1 [mm]
h	enthalpy [J kg^{-1}]
h_c	heat transfer coefficient [W m^{-2} K^{-1}]
h_{lg}	latent heat of evaporation [J kg^{-1}]
h_{sl}	latent heat of melting [J kg^{-1}]
j	evaporation rate [kg m^{-2} s^{-1}]
k_i	thermal conductivity, k_l or k_s [W m^{-1} K^{-1}]
p	vapour pressure [Pa]
q	maximum incident energy flux, $Q/2\pi\sigma^2$ [W m^{-2}]
Q	beam power [W]
Q_i	total incident energy on an area of radius r_0 near cavity base, defined in equation (10) [W]
Q_r	total radial heat conduction across liquid layer, defined in equation (10) [W]
r, R	dimensional and dimensionless radial coordinate, $R = r/\sigma$, as illustrated in Fig. 1
R_g	specific gas constant [J kg^{-1} K^{-1}]
r_0	0.00625 mm
R_1, R_2	principal curvatures of vapour–liquid interface [m]
T	temperature [K]
u	penetration velocity [m s^{-1}]
z, Z	dimensional and dimensionless vertical coordinate, $Z = z/\sigma$, as illustrated in Fig. 1.

Greek symbols

α, β	accommodation coefficient for evaporation rate and pressure
γ	surface tension, $\gamma_m + (d\gamma/dT)(T - T_m)$ [N m^{-1}]
δ	liquid layer thickness at cavity base [mm]
ε	half temperature range used for smoothing discontinuity of enthalpy across liquid–solid interface, 0.001 K
θ	dimensionless temperature, T/T_m
Λ	$k_l T_m \sigma / Q$
ρ	density [kg m^{-3}]
σ	energy distribution parameter [mm].

Subscripts

b	boiling
l	liquid
m	melting
s	solid
∞	ambient.

power. It was also shown in ref. [2] that the energy distribution parameter has the most significant effects on the geometry and temperatures of the welding cavity. To simplify the model of the drilling process, the shape of the liquid–solid interface and the penetration velocity, which were assumed to be independent of the incident energy flux were specified in ref. [9]. In view of this inappropriate assumption, a more relevant relationship between the beam characteristics with the penetration velocity is needed. This is the objective of the present work.

In this study, effects of the beam power and the energy distribution on the high-energy beam drilling process are examined. The normal pressure condition at the vapour–liquid interface is used to determine the shape of the vapour–liquid interface. Although the flow of the liquid layer is responsible for the formation of the cavity, heat convected by the liquid can be neglected without significant errors [13]. The reason for this is that the tangential velocity of the liquid layer is roughly 1 m s^{-1} near the cavity base of radius of around 0.1 mm [9]. Therefore, the Peclet number for copper can be estimated to be around 2 near the bottom of the cavity considered. The heat conduction in both the axial and the radial directions, heats of evaporation and melting are taken into account. The fusion line, however, is calculated by using the enthalpy method [14]. This study will provide an evaluation on heat transfers which will be important to understand the high-energy beam drilling process.

ANALYSIS

A thin layer of molten metal flows along the wall near the base of a vapour-filled cavity as illustrated in Fig. 1. An rz coordinate system is assumed to move into the solid at a steady penetration velocity, which is relevant for penetrating times greater than 0.1 μs, as shown by the measurements of von Allmen [11] and Arata and Miyamoto [15]. The penetrating process is thus simplified to an axisymmetric, quasi-steady state in this moving coordinate system. The incident energy density can be assumed to be a Gaussian distribution, as measured by Burgardt [16]. At the vapour–liquid interface the force due to the surface tension, which is responsible for the fluid flow of the liquid layer [8, 9], is taken into account to balance the vapour pressure. Assuming that the penetration depth is not large, the hydrostatic pressure can be neglected. The effect of heat convection can be assumed to be negligible near the cavity base as discussed previously. The energy transfer across the fusion zone, being partially dissipated by the heat conduction in the radial

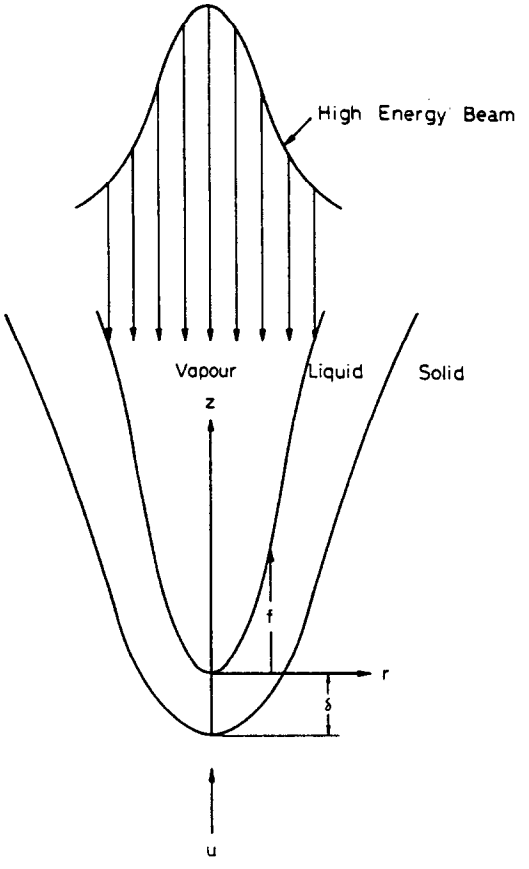

FIG. 1. Schematic sketch of high-energy density beam penetrating process and coordinate system.

direction, melts the solid material and produces a heat-affected zone.

Governing equations and boundary conditions

One of the difficulties associated with the phase change problem is a determination of the shape of the fusion line. Neither the heat fluxes, the velocity of the interface, nor the interface location itself are known a priori. To predict the shape of the fusion zone, the enthalpy method described by Crank [14] can be effectively used. Instead of working entirely in terms of the temperature of the heat conduction equation, an enthalpy function which represents the total heat content of the material is introduced. With a correct enthalpy–temperature relation, the full effect of the phase change can be modelled without a need to know the exact position of the phase change region. This makes the numerical technique relatively easy. In this study the enthalpy formulation of the heat conduction equation in the quasi-steady state applied to both the molten and the heat-affected zones of the workpiece can be simply represented by

$$\rho u \frac{\partial h}{\partial z} = \frac{1}{r}\frac{\partial}{\partial r}\left(k_i r \frac{\partial T}{\partial r}\right) + \frac{\partial}{\partial z}\left(k_i \frac{\partial T}{\partial z}\right) \qquad (1)$$

where u, the penetration velocity of the cavity, is assumed to be a constant, k_i represents liquid and solid thermal conductivities k_l and k_s, respectively. The enthalpy h is defined by

$$h = \begin{cases} c_s T, & T < T_m - \varepsilon \\ c_s T + \dfrac{h_{sl}}{2\varepsilon}(T - T_m + \varepsilon), & T_m - \varepsilon \leqslant T \leqslant T_m + \varepsilon \\ c_l T + h_{sl}, & T_m + \varepsilon < T \end{cases} \qquad (2)$$

where equation (2) was originally proposed by Meyer [17] for the purpose of smoothing the enthalpy which is a discontinuous function across the solid–liquid interface for a pure substance undergoing a change of phase. Hence, a small value of ε (e.g. 0.001 K) is assumed for the numerical modelling in this study.

The beam energy is balanced with the heat conduction and the energy due to evaporation at the vapour–liquid interface and yields

$$\frac{Q}{2\pi\sigma^2}\exp\left(-\frac{r^2}{2\sigma^2}\right) = -k_l\left(\frac{\partial T}{\partial r}\frac{\mathrm{d}f}{\mathrm{d}r} - \frac{\partial T}{\partial z}\right) + j h_{lg}\left[1 + \left(\frac{\mathrm{d}f}{\mathrm{d}r}\right)^2\right]^{1/2} \qquad (3)$$

where σ is the energy distribution parameter that defines the region in which 39% of the total heat is deposited. The function f denotes the location of the vapour–liquid interface as illustrated in Fig. 1. Heat-conduction loss to the vapour can be neglected since thermal conductivity of the gas is much smaller than that of the liquid. The evaporation rate j can be determined from the equilibrium equation developed by Langmuir [18]

$$j = \frac{\alpha p_b}{\sqrt{(2\pi R_g T)}}\exp\left[\frac{h_{lg}}{R_g}\left(\frac{1}{T_b} - \frac{1}{T}\right)\right]. \qquad (4)$$

The accommodation coefficient $\alpha = 0.816$ given by Knight [19] was found to account for the back-scattering of evaporating atoms for a strong evaporation. The Stefan boundary condition evaluated at $r = 0$ on the liquid–solid interface can be used to determine the penetration velocity

$$u = \frac{1}{\rho h_{sl}}\left(k_l \left.\frac{\partial T}{\partial z}\right|_{z=-\delta^+} - k_s \left.\frac{\partial T}{\partial z}\right|_{z=-\delta^-}\right). \qquad (5)$$

Boundary conditions in the z-direction are

$$-k_l \frac{\partial T}{\partial z} = h_c(T - T_\infty) \quad \text{at} \quad z = 3\sigma \qquad (6)$$

$$k_s \frac{\partial T}{\partial z} = h_c(T - T_\infty) \quad \text{at} \quad z = -3\sigma \qquad (7)$$

where $z = \pm 3\sigma$ indicates that the region considered in this study is approximately within two times the diameter of the energy beam near the cavity base. Boundary condition (6) is introduced to remove com-

plicated phenomena occurring near the top of the workpiece by choosing an appropriate value of h_c. Errors caused by this assumption will not be significant since heat transferred is primarily in the radial direction far from the cavity base, as can be verified later by investigating the temperature field. The axisymmetric condition is satisfied at $r = 0$

$$\frac{\partial T}{\partial r} = 0. \tag{8}$$

The solid remains at the ambient temperature T_∞ as $r \to \infty$.

An additional boundary condition is needed to determine the shape of the cavity. The effective surface pressure is balanced with the surface tension [9]

$$\beta p_b \exp\left[\frac{h_{lg}}{R_g}\left(\frac{1}{T_b} - \frac{1}{T}\right)\right] = \gamma\left(\frac{1}{R_1} + \frac{1}{R_2}\right) \tag{9}$$

where $\beta = 0.55$ was calculated by Knight [19] by taking into account the effect of thermodynamic non-equilibrium at the evaporating surface. The surface tension is assumed to be a linear function of temperature and varies along the free surface of the liquid layer.

The ratio of the total radial heat conduction across the liquid layer to the beam energy incident on a small area of radius r_0 at the cavity base can be calculated

$$\frac{Q_r}{Q_i} = \frac{\int_{-\delta}^{0} -k_l \frac{\partial T}{\partial r} 2\pi r_0 \, dz}{\int_0^{r_0} \frac{Q}{2\pi\sigma^2} \exp\left(-\frac{r^2}{2\sigma^2}\right) 2\pi r \, dr}. \tag{10}$$

Numerical procedure

The discrete form of equation (1) with boundary conditions (3), (5)–(9) was obtained by using the central finite differences. A grid of 40×30 nodal points ensured independence of the solution on the grid. The nodal points in both the r- and z-directions were non-uniformly distributed and had a greater concentration of points near the vapour–liquid interface. For comparison with the experimental results, a grid of 95×42 nodal points was used. The key steps for solving this problem are as follows.

(1) Shapes of the cavity and one penetration velocity which satisfies the Stefan boundary condition equation (5) were guessed for a given beam power and an energy distribution parameter.

(2) The enthalpy equation (1) was solved with boundary conditions (5)–(9) by using the successive overrelaxation method [20] with a relaxation factor of 1.25 until the temperature converged to a relative error limit of 0.5%.

(3) An appropriate shape of the cavity was determined from the energy equation (3) by using the method developed by Wei and Giedt [8] with a relative error of less than 6%. Otherwise, another penetration velocity was guessed and steps 1–3 were repeated.

RESULTS AND DISCUSSION

The workpiece is chosen to be copper (Table 1) in order to compare it with experimental data obtained by von Allmen [11]. For clarity, most of the figures are provided in dimensional coordinates to quantify physical phenomena during a high-energy beam penetrating process.

Temperature profiles in the bulk material along the axisymmetric axis for different energy distribution parameters and beam powers are shown in Fig. 2. The cavity base temperatures are relatively constant with values around 2985 K. This result agrees with the conclusion drawn in refs. [2, 21]. The radiative energy loss can be estimated to be around 0.5% of the beam power of 3 kW at a cavity opening radius of 1 mm and surface temperature of 3000 K. Hence, energy loss due to radiation can be neglected. The location of the melting temperature 1357 K determines the liquid layer thickness. The liquid layer thickness decreases from 0.0085 to 0.0075 mm as the beam power increases from 2.61 to 3.05 kW at an energy distribution parameter of 0.083 mm, while an increase from 0.0075 to 0.0096 mm is obtained as the energy distribution parameter increases from 0.083 to 0.1 mm at a beam power of 3.05 kW. This indicates that variations in the energy distribution have a stronger effect on cavity drilling than the beam power. Hence, the liquid layer thickness of 0.1 mm found by Wei and Chiou [9] for drilling aluminium at an energy distribution parameter of 1 mm is possible.

Ratios of the radial heat conduction to the total beam energy incident on a small area of radius 0.00625 mm at the cavity base for different energy distribution parameters and beam powers are shown in Fig. 3. The radial heat conduction-to-incident energy ratio increases from 0.39 to 0.48 as the beam power increases from 1.5 to 3 kW at an energy distribution parameter of 0.083 mm. Similarly, an increase of the radial heat conduction-to-incident energy ratio from 0.3 to 0.46 is obtained at an energy distribution parameter of 0.1 mm. This indicates that radial heat conduction loss cannot be neglected for an energy beam of a high beam power or a small energy distribution parameter.

Table 1. Properties of copper

Density, ρ (kg m^{-3})	8300
Solid conductivity, k_s (W m^{-1} K^{-1})	270
Liquid conductivity, k_l (W m^{-1} K^{-1})	190
Solid specific heat, c_s (J kg^{-1} K^{-1})	450
Liquid specific heat, c_l (J kg^{-1} K^{-1})	495
Latent heat of evaporation, h_{lg} (J kg^{-1})	4.8×10^6
Latent heat of melting, h_{sl} (J kg^{-1})	2.05×10^5
Melting temperature, T_m (K)	1357
Surface tension at melting temperature, γ_m (N m^{-1})	1.285
Surface tension coefficient, $d\gamma/dT$ (N m^{-1} K^{-1})	-1.3×10^{-4}

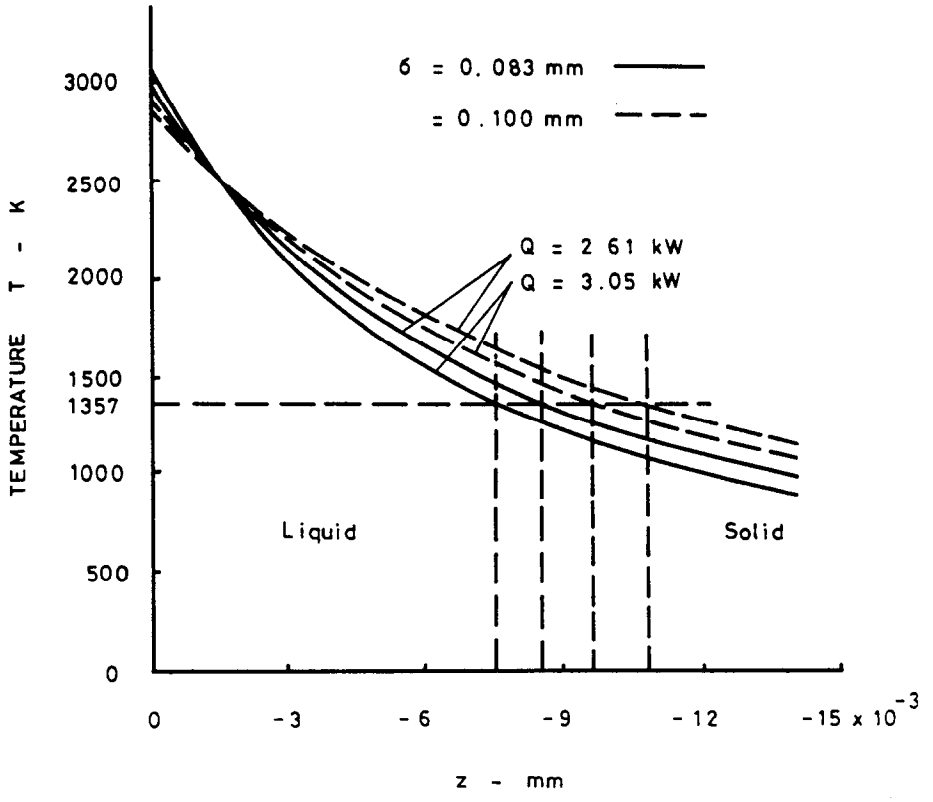

FIG. 2. Temperature profiles along axisymmetric axis for different energy distribution parameters and beam powers for drilling copper.

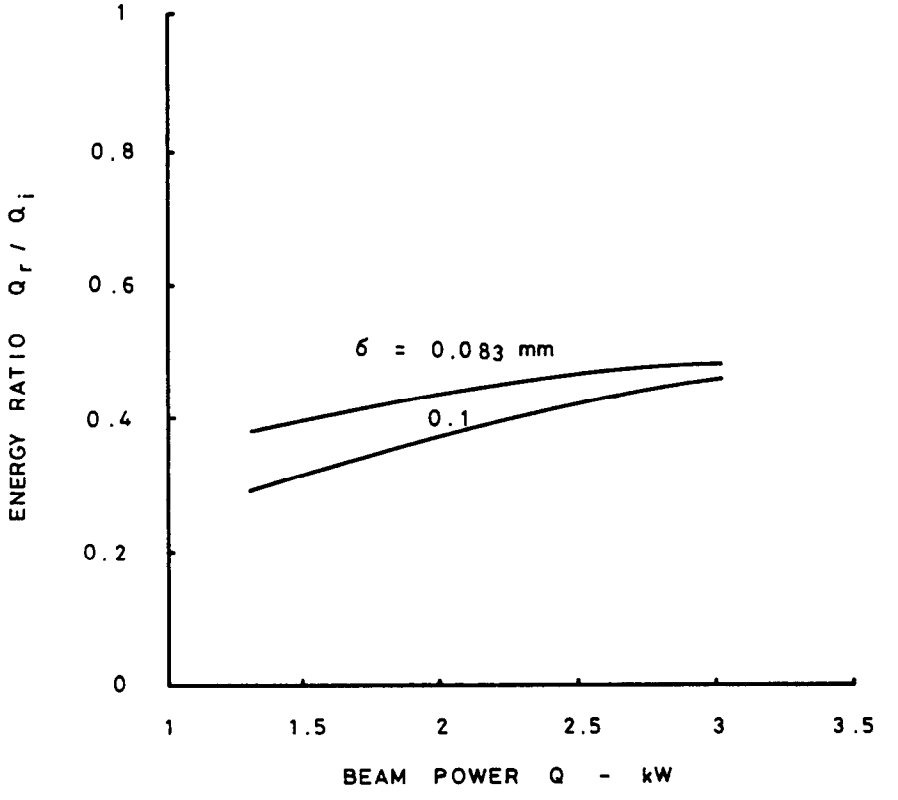

FIG. 3. Variation in ratio of total radial heat conduction to beam energy incident on a small area of radius of 0.00625 mm near the cavity base with beam power for different energy distribution parameters for drilling copper.

Variations of heat transfers with the maximum energy flux incident on the cavity base are shown in Fig. 4 for an energy distribution parameter of 0.083 mm. By linearly extrapolating below 3×10^{10} W m^{-2}, the evaporation rate can be estimated to be around 1×10^{-7} kg s^{-1}, which is of the same magnitude as the experimental data obtained by Schwarz [22] for drilling copper at a beam power of 1.44 kW and an electron beam diameter of 0.2 mm. The ratio of evaporation to melting rates is roughly 2%. Hence, most of the mass melted is convected upwards along the cavity wall and produces a cavity as interpreted by Wei and Chiou [9]. If the formation of a cavity was due to pure evaporation proposed by the one-dimensional penetration model, the solid material completely evaporated would have to be 50 times larger than the experimental data. This results in a significant overestimation of the energy due to evaporation. In view of neglecting the radial heat conduction loss and overestimating the energy required for evaporation, the one-dimensional heat conduction penetration models [5, 10] are inherently invalid. In the present work the energy loss due to evaporation is found to be only 2% of the maximum incident energy density in the range below 7×10^{10} W m^{-2}. This confirms the estimations made by Hashimoto and Matsuda [23] and Wei and Chiou [9].

The incident beam energy can be dissipated by energy losses due to evaporation, radiation, an increase in the internal energy of the workpiece from the melting temperature to the cavity base temperature, latent heat for melting and heat conduction to the surroundings in both the radial and axial directions. For simplicity, heat convected by the flow of the liquid layer can be neglected, as discussed previously. In this study the ratio of the energy density transferred to the liquid–solid interface to the maximum incident energy flux for an energy flux near 7×10^{10} W m^{-2} is found to remain a relative constant of 0.45, which corresponds to 48% of an energy beam of 3 kW incident on a small area of radius of 0.00625 mm. Since the radial heat conduction loss is 45% of the incident energy (refer to Fig. 3) and the energy loss due to evaporation is 2%, the energy required to raise the liquid from the melting temperature to the maximum temperature of 3000 K will only be 5% of the incident energy. The melting energy-to-incident energy density ratio can also be found to remain relatively constant at a value of 3%.

Energy transfers and the liquid layer thickness at a higher energy distribution parameter of 0.1 mm are shown in Fig. 5. Since the ratio of the energy for melting to the incident energy flux is approximately a constant, it indicates that the energy required for

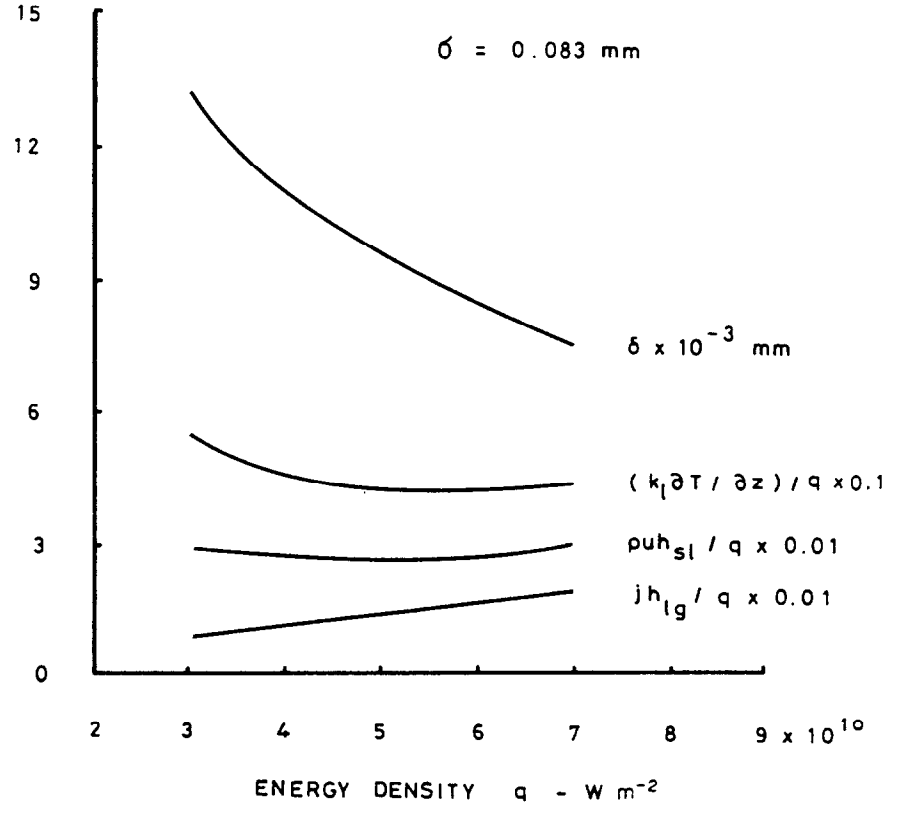

FIG. 4. Variation in heat transfers and liquid layer thickness with energy flux incident on cavity base for an energy distribution parameter of 0.083 mm for drilling copper.

melting increases linearly with the incident energy flux. A comparison of the calculated penetration velocities with the experimental data obtained by von Allmen [11] is shown in Fig. 6. At an energy distribution parameter of 0.083 mm the penetration velocity increases with the beam power. The consistency observed demonstrates that the penetrating process can be appropriately investigated by neglecting effects of evaporation. Referring to Figs. 3 and 4, it is found that when the incident energy density is doubled via increasing the beam power, an increase in the radial conduction loss is only 39–48%. Since the energy required to raise the liquid from the melting temperature to 3000 K is usually around 5%, the heat transfer to melt the solid increases and results in a significant increase in the penetration velocity.

The variation in the penetration velocity with the beam power for different energy distributions is shown in Fig. 7. Decreasing the energy distribution parameter or increasing the beam power results in an increase in penetration velocity. The energy distribution parameter is found to have a stronger effect on the penetration velocity than the beam power. A significant increase in the penetration velocity initiates earlier at either a higher beam power or a smaller energy distribution parameter.

Typical temperature distributions for different liquid heat conduction-to-beam power parameters in a workpiece are shown in Fig. 8. The very close spacing in front of the cavity indicates a region of high temperature gradients and high heat transfer rates. The region between the cavity and the isothermal line $\theta = 1$ represents the fusion zone. It can be seen that a narrower cavity is produced at a lower liquid heat conduction-to-beam power parameter due to an increase in the heat flux near the cavity axis. Since the temperature gradient is much higher in the radial direction than in the vertical direction, heat transfer in the upward direction far from the cavity base has little effect on the penetrating process. As a result, the use of the boundary condition (6) is relevant.

CONCLUSIONS

The conclusions drawn are as follows.

(1) In this study, a quasi-steady, axisymmetric heat conduction model is developed to investigate the penetrating process of the cavity produced by a high-energy beam. The shape of the fusion zone and the penetration velocity are determined as a function of the energy distribution parameter and the beam power, rather than specified a priori. Results show that the energy distribution parameter has stronger

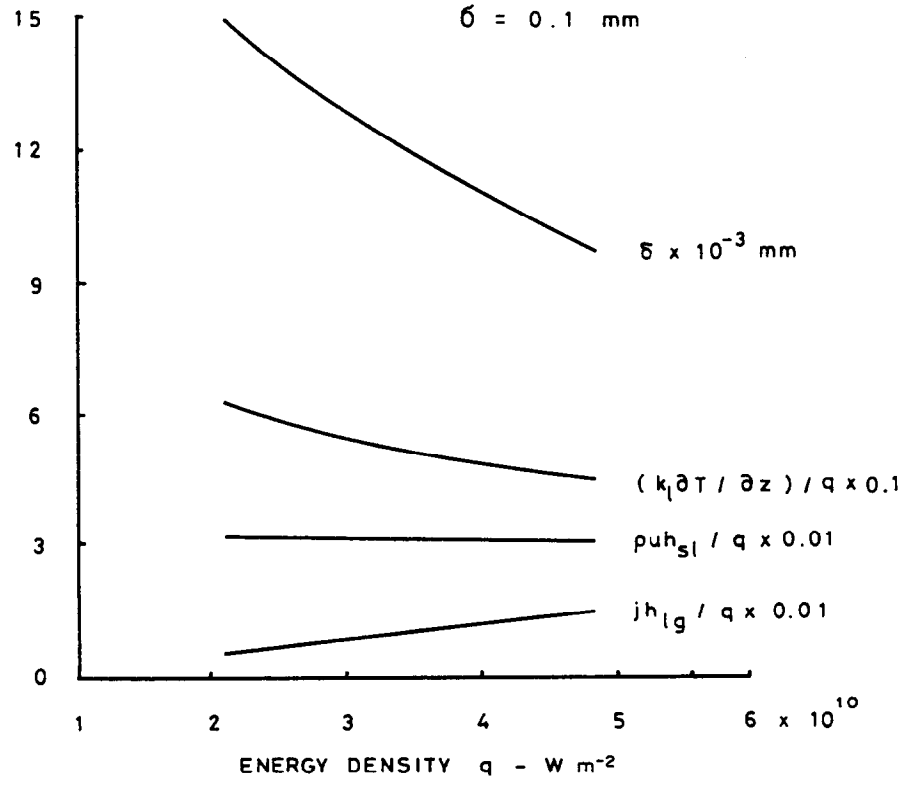

FIG. 5. Variation in heat transfers and liquid layer thickness with energy flux incident on cavity base for an energy distribution parameter of 0.1 mm for drilling copper.

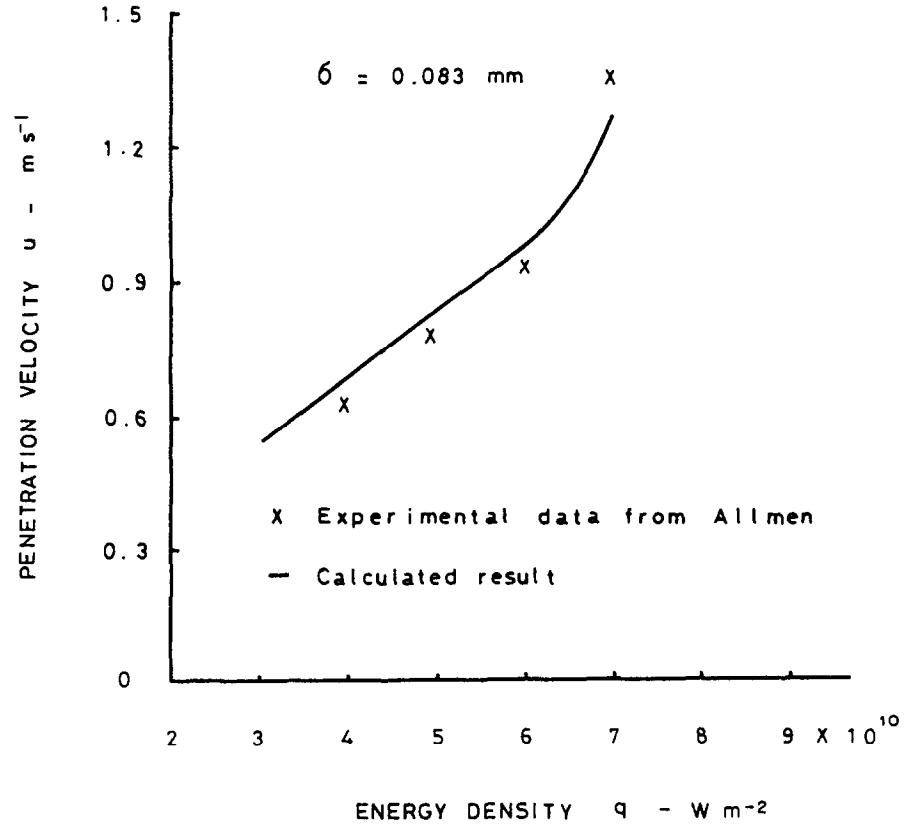

FIG. 6. Comparison between the calculated and measured penetration velocities vs beam-energy flux for an energy distribution parameter of 0.083 mm for drilling copper.

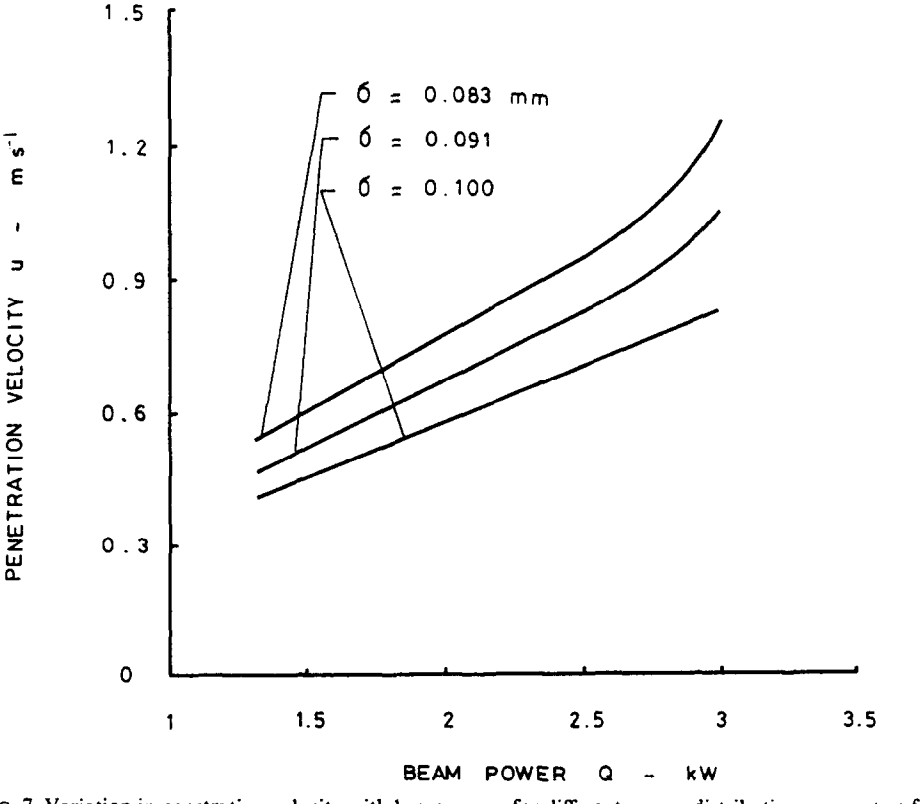

FIG. 7. Variation in penetration velocity with beam power for different energy distribution parameters for drilling copper.

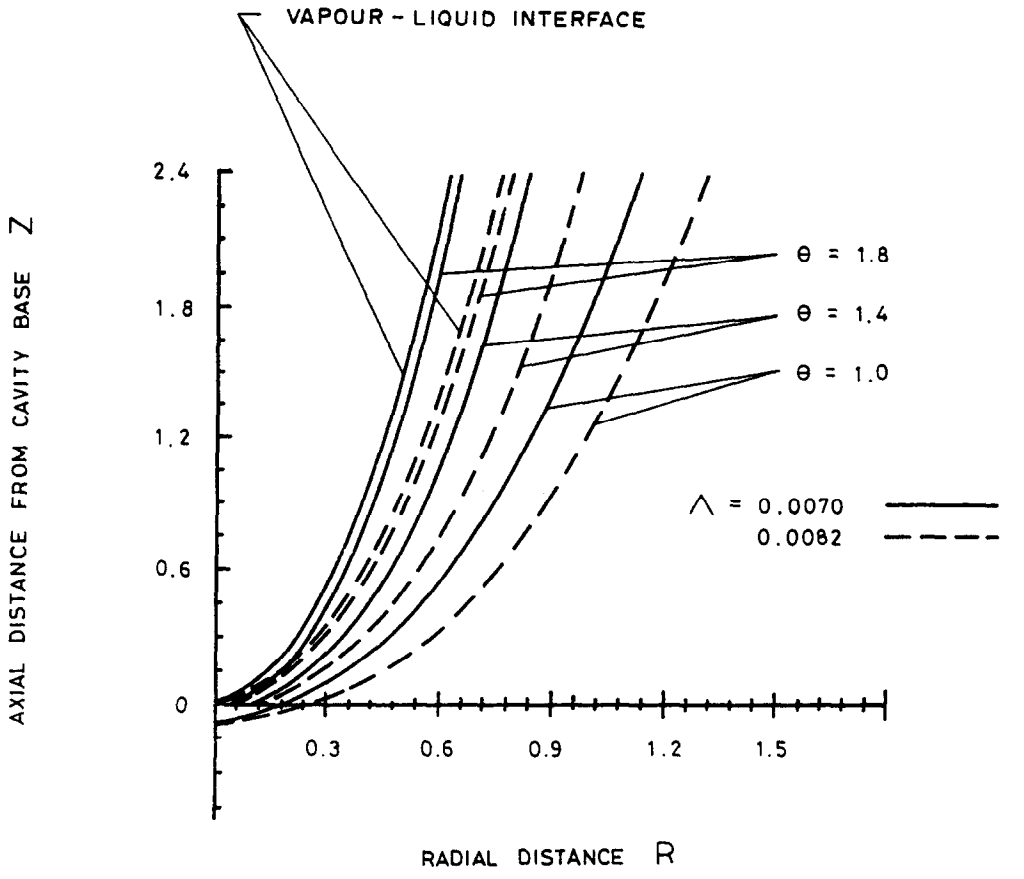

FIG. 8. Dimensionless temperature field and shape of cavity for different liquid heat conduction-to-beam power parameters.

effects than the beam power on the high-energy beam drilling or welding process.

(2) Assuming that energy convected by the liquid layer can be neglected since the Peclet number is around 2 near the cavity base, heat transfers for drilling copper with a high-energy beam are calculated. Primary energy losses are due to axial and radial heat conduction, which may be 40–50% of the beam energy for a high beam power or a small energy distribution parameter. The heat required for melting or evaporation is only 2–3% for an energy density below 7×10^{10} W m^{-2}, while the sensible heat of raising the liquid from the melting temperature to 3000 K at the cavity base is roughly 5%. The radiative energy loss can be estimated to be around 0.5%.

(3) The evaporation rate calculated is around 1×10^{-7} kg s^{-1}, which is of the same order as the experimental data. If the formation of the high-energy beam cavity were due to pure evaporation, the evaporation rate would be 50 times larger than experimental findings. On the other hand, significant radial heat conduction loss of around 50% will occur if the energy distribution parameter decreases or the beam power increases. Consequently, using the conventional one-dimensional, pure evaporation model to investigate the drilling process is inherently invalid.

(4) The penetration velocity increases with increasing beam power or decreasing energy distribution parameter. Increasing the energy flux results in a slight increase in radial conduction loss. Since the sensible heat of raising the liquid from the melting temperature to the base temperature is small, the energy transferred to the liquid–solid interface becomes larger for a higher energy flux. This results in a non-linear and significant increase in the penetration velocity at a high beam power or a small energy distribution parameter.

(5) High temperature gradients occur near the cavity base. Decreasing the liquid heat conduction–beam power parameter induces a narrower cavity.

(6) An appropriate evaluation of the relative magnitudes of energy transfer provided by this study will be useful for a quantitative understanding of the complicated high-energy beam penetrating process.

REFERENCES

1. H. Tong and W. H. Giedt, Depth of penetration during electron beam welding, *J. Heat Transfer* 93, 155–163 (1971).
2. P. S. Wei, T. H. Wu and Y. T. Chow, Investigation

of high-intensity beam characteristics on welding cavity shape and temperature distribution, *J. Heat Transfer* **112**, 163–169 (1990).
3. V. I. Leskov, E. N. Trunov and L. I. Zhivada, Mechanism in deep weld pools during electron-beam welding, *Avt. Svarka* **1**, 12–15 (1975).
4. N. Rykalin, A. Uglov and A. Kokora, *Laser Machining and Welding* (English translation), p. 126. Mir (1978).
5. J. F. Ready, Effects due to absorption of laser radiation, *J. Appl. Phys.* **36**, 462–468 (1965).
6. L. P. Connor (Editor), *Welding Handbook* (8th Edn), Vol. 1, p. 40. American Welding Society, Miami (1987).
7. N. A. Ol'Shanskii, Movement of molten metal during electron beam welding, *Svar. Proiz.* **21**, 12–14 (1974).
8. P. S. Wei and W. H. Giedt, Surface tension gradient-driven flow around an electron beam welding cavity, *Welding J.* **64**, 251-s–259-s (1985).
9. P. S. Wei and L. R. Chiou, Molten metal flow around the base of a cavity during a high-energy beam penetrating process, *J. Heat Transfer* **110**, 918–923 (1988).
10. A. V. Luikov, T. L. Perelman and S. I. Anisimov, Evaporation of a solid into vacuum, *Int. J. Heat Mass Transfer* **14**, 177–184 (1971).
11. M. von Allmen, Laser drilling velocity in metals, *J. Appl. Phys.* **47**, 5460–5463 (1976).
12. W. H. Giedt and L. N. Tallerico, Prediction of electron beam depth of penetration, *Welding J.* **67**, 299-s–305-s (1988).
13. W. H. Giedt and P. S. Wei, Temperature and velocity distributions in the liquid flowing around the front of an electron beam welding cavity, *Proc. 7th Int. Heat Transfer Conf.*, Vol. 6, pp. 403–407. Hemisphere, Washington, DC (1982).
14. J. Crank, *Free and Moving Boundary Problems*, Chap. 6. Clarendon Press, Oxford (1984).
15. Y. Arata and I. Miyamoto, Processing mechanism of high energy density beam (Report I)—mechanism of drilling, *Trans. JWRI* **2**, 19–22 (1973).
16. P. Burgardt, Electron beam size calibration, *Summary of Calibration of Welding Systems Meeting* (Edited by L. N. Tallerico), pp. 258–266. Sandia National Lab., Livermore, California (1986).
17. G. H. Meyer, Multidimensional Stefan problems, *SIAM J. Numer. Analysis* **10**, 522–538 (1973).
18. I. Langmuir, The vapor pressure of metallic tungsten, *Phys. Rev.* **2**, 329–342 (1913).
19. C. J. Knight, Transient vaporization from a surface into vacuum, *AIAA J.* **20**, 950–954 (1982).
20. S. V. Patankar, *Numerical Heat Transfer and Fluid Flow*, p. 67. McGraw-Hill, New York (1980).
21. D. A. Schauer, W. H. Giedt and S. M. Shintaku, Electron beam welding cavity temperature distributions in pure metals and alloys, *Welding J.* **57**, 127-s–133-s (1978).
22. H. Schwarz, Mechanism of high-power-density electron beam penetration in metal, *J. Appl. Phys.* **35**, 2020–2029 (1964).
23. T. Hashimoto and F. Matsuda, Penetration mechanism of weld beads in electron-beam welding—studies on EB weldings No. 6, *Trans. Natn. Res. Inst. Metals* **7**, 183–185 (1965).

CONSIDERATIONS ENERGETIQUES SUR LE PERCAGE PAR UN FAISCEAU A HAUTE ENERGIE

Résumé—On détermine les transferts d'énergie et la vitesse de pénétration pendant le perçage à haute énergie ou le soudage. L'énergie du faisceau à distribution gaussienne, à la surface libre de la couche liquide qui sépare le solide non fondu et la vapeur, est égale à la somme de la chaleur conductive et des chaleurs latentes de fusion et d'évaporation. Les formes des interfaces vapeur–liquide et liquide–solide ainsi que la vitesse de pénétration sont déterminées en fonction de la distribution d'énergie et de la puissance du faisceau. La chaleur transférée par convection est négligée à cause du petit nombre de Peclet proche de 2 près du fond de la cavité. Les résultats montrent que la variation non linéaire de la vitesse de pénétration avec la densité d'énergie pour un flux d'évaporation de l'ordre de 1×10^{-7} kg s^{-1} s'accorde avec les données expérimentales pour le perçage du cuivre. L'énergie nécessaire pour la fusion et l'évaporation est seulement 2–3% de l'énergie incidente de l'ordre de 7×10^{10} W m^{-2}. Le modèle monodimensionnel d'évaporation conventionnelle n'est pas valable pour prédire la pénétration à cause d'une surestimation significative du taux d'évaporation et d'une perte de conduction radiale proche de 50%.

ENERGETISCHE BETRACHTUNG DES BOHRENS MIT HOCHENERGIESTRAHLEN

Zusammenfassung—Es wird die Energieübertragung und die Eindringgeschwindigkeit beim Bohren oder Schweißen mit Hochenergiestrahlen untersucht. Der Energiestrahl fällt entsprechend einer Gauß'schen Verteilung auf die freie Oberfläche einer Flüssigkeitsschicht, die ungeschmolzenen Feststoff und Dampf voneinander trennt. Diese einfallende Energie steht im Gleichgewicht mit der Wärmeleitung und mit der Schmelz- und Verdampfungswärme. Die Form der Dampf/Flüssigkeits-Grenzfläche und der Flüssigkeits/Feststoff-Grenzfläche sowie die Eindringgeschwindigkeit werden in Abhängigkeit der Energieverteilung und der transportierten Leistung untersucht. Aufgrund der kleinen Peclet-Zahl (ungefähr 2 am Schmelzgrund) kann der konvektive Wärmetransport vernachlässigt werden. Die Ergebnisse, welche bei einer Verdampfungsgeschwindigkeit der Größenordnung 10^{-7} kg s^{-1} für die nicht-lineare Abhängigkeit der Eindringgeschwindigkeit von der Energiedichte ermittelt werden, stimmen gut mit Versuchsdaten für das Bohren in Kupfer überein. Im Bereich unterhalb 7×10^{10} W m^{-2} beträgt die Energie für das Schmelzen oder Verdampfen nur 2 – 3% der einfallenden Energie. Das herkömmliche Modell, das reine Verdampfung und eindimensionales Eindringen berücksichtigt, ist wegen einer beachtlichen Überbewertung der Verdampfungsrate und nahezu 50% radialen Wärmeverlusten weitgehend ungültig.

ЭНЕРГЕТИЧЕСКИЙ АСПЕКТ ПРОЦЕССА ИНТЕНСИВНОГО ЛУЧЕВОГО ПРОПЛАВЛЕНИЯ ОТВЕРСТИЙ

Аннотация—Исследуется перенос энергии и скорость проникновения в процессе проплавления или сварки. Выводится баланс между энергией гауссова пучка, падающего на свободную поверхность слоя жидкости, которая разделяет нерасплавленное тело и пар, и теплопроводностью и скрытой теплотой в случае плавления и испарения. Формы границ раздела пар–жидкость и жидкость–твердое тело, а также скорость проникновения определяются как функция распределения энергии и мощности пучка. Конвективный теплоперенос не учитывается из-за малых значений числа Пекле, составляющих приблизительно 2 вблизи основания полости. Результаты показывают, что нелинейное изменение скорости проникновения с изменением плотности энергии и скорость испарения порядка 1×10^{-7} кг $с^{-1}$ согласуются с экспериментальными данными для проплавляющей меди. Энергия, необходимая для плавления или испарения, составляет Только 2–3% от энергии падающего пучка в диапазоне ниже 7×10^{10} Вт $м^{-2}$. Обычная одноменая модель проникновения с испарением является непригодной, так как она значительно завышает скорость испарения и приводит почти к 50% радиальных потерь тепла теплопроводностью.